Accepted Manuscript

Experimental and numerical investigations of the electro-viscoelastic behavior of VHB 4905^{TM}

Markus Mehnert, Mokarram Hossain, Paul Steinmann

PII: S0997-7538(18)30996-3

DOI: https://doi.org/10.1016/j.euromechsol.2019.103797

Article Number: 103797

Reference: EJMSOL 103797

To appear in: *European Journal of Mechanics / A Solids*

Received Date: 20 December 2018

Revised Date: 16 April 2019

Accepted Date: 26 May 2019

Please cite this article as: Mehnert, M., Hossain, M., Steinmann, P., Experimental and numerical investigations of the electro-viscoelastic behavior of VHB 4905^{TM}, *European Journal of Mechanics / A Solids* (2019), doi: https://doi.org/10.1016/j.euromechsol.2019.103797.

Experimental and Numerical Investigations of the Electro-Viscoelastic Behavior of VHB 4905™

Markus Mehnert, Mokarram Hossain and Paul Steinmann

Abstract Dielectric elastomers are a class of electro-active polymers (EAPs) that can be used for the development of simple soft actuators, sensors and energy harvesters. Their operation principle is based on the interaction of quasi-static electric charges in combination with soft dielectrics and deformable electrodes. Due to their ability to undergo large deformations with a time dependent material response of the underlying polymer, the mechanical behaviors of EAPs can be described by a finite strain viscoelastic material model [1]. This model is here augmented in order to account for the influence of the electro-mechanical coupling. In this contribution we persue a comprehensive electro-mechanical characterization of the popular dielectric polymer VHB 4905™. In contrast to the results of the electro-mechanical experiments published previously [2] all of these experiments are conducted without the application of a pre-stretch and are therefore well suited for the identification of the coupling parameters of the material model. The presented model shows excellent agreements with experimental findings.

Markus Mehnert
Chair of Applied Mechanics, University of Erlangen-Nuremberg, Egerlandstr. 5, 91058 Erlangen, Germany, e-mail: markus.mehnert@fau.de

Paul Steinmann
Chair of Applied Mechanics, University of Erlangen-Nuremberg, Egerlandstr. 5, 91058 Erlangen, Germany e-mail: paul.steinmann@fau.de
Glasgow Computational Engineering Centre (GCEC), University of Glasgow, United Kingdom

Mokarram Hossain
Zienkiewicz Centre for Computational Engineering, College of Engineering, Bay Campus, Swansea University, Swansea, UK e-mail: mokarram.hossain@swansea.ac.uk

1 Introduction

When dielectric elastomers are used as electro-active materials their principle of operation is based on the attraction of opposite electric charges and the repulsion of like charges. A simple way to design a soft actuator using this class of materials is to sandwich a polymeric thin film between deformable electrodes. When a voltage difference is applied between the electrodes, the opposite charges will attract each other resulting in a force that contracts the thin film. Simultaneously the like charges on each electrode generate a force that stretches the material in the in-plane directions, compare Figure 1.

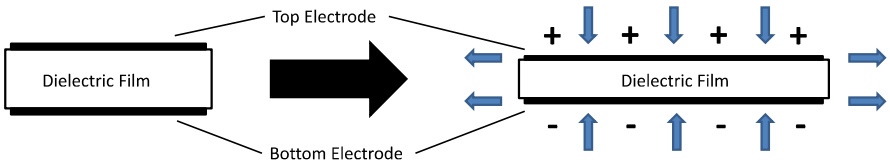

Fig. 1 Working principle of a simple soft actuator of dielectric elastomer with an electrically conductive coating in the undeformed state (left) and in the activated state (right). The blue arrows indicate the electric stress resulting from the electric charges.

Using this basic principle, dielectric elastomer transducers can be designed in a number of ways, e.g. as rigid or flexible framed planar transducers, bending, rolled or tubular transducers or in form of a diaphragm [3]. This wide range of possible designs makes dielectric elastomers as interesting candidates for numerous application areas such as adaptable optics where they can be used as tune-able lenses [4] or laser speckle reducers [5], microfluidic pumping systems [6, 7] or as artificial muscles, especially in the field of biomimetics [8, 9, 10, 11, 12, 13]. The traditional options for the dielectric base material include silicones, acrylic copolymers and polyurethanes [14, 15] whereas the conventional choices for the material of the electrodes includes carbon based powders, greases [16] or metallic thin films [17, 18, 19].

The numerical simulation taking into account the interaction between a body and an electric field has been the subject of intensive research, beginning with early attempts by e.g. Eringen [20], Allik and Hughes [21] or Kagawa and Ymabuchi [22]. The growing interests in electro-active materials have led to a number of advances in the past decade with important contributions by Dorfmann and Ogden [23, 24, 25] among others. For polymeric materials in particular, a time dependent material response has to be considered for which phenomenological or micro-mechanical constitutive models have been developed over the years. Furthermore these models can be characterized by the nature of the time-dependent contribution of the stress

which contains either stress-type internal variables [26, 27, 28] or strain-type internal variables [29, 30]. The fields of electro-mechanics and viscoelasticity were successfully combined for the simulation of electro-active polymers, for example in the works of Ask et al. [31, 32], Buschel et al. [33] or Saxena et al. [34]. However, a central issue of these theoretical approaches is a lack of reliable experimental data suited for the identification of both the purely mechanical material parameters and the electro-mechanical coupling parameters. In one of the few contributions, Hossain et al. [35] carefully analyzed the visco-mechanical material response of the dielectric elastomer VHB 4910^{TM} by 3M^{TM} by performing a number of standard and relevant experiments such as single- and multi-step relaxation tests and cyclic loading-unloading tests. These experiments were used for the identification of the material parameters of a micro-mechanically motivated viscoelastic material model resulting in a very good agreement between the simulation and the experimental results. In a subsequent contribution, Hossain et al. [2] also investigated the electro-mechanical response of the same material. However, in the electro-mechanically coupled experimentations, the polymeric samples were pre-stretched manually in an effort to reduce their initial thickness of 1 mm and by this amplify the effect of the electric field on the material. This leads to experimental results that were not well suited for the identification of relevant material parameters appearing in an electro-viscoelastically coupled constitutive model where the electric field is an independent field in addition to a mechanical load. Moreover, any kind of pre-stretching reduces the service life of dielectric elastomers. Hence, it would be a better option if thinner samples can be obtained that will show good actuation behaviour without any pre-stretching.

Within the current contribution we are trying to fill this gap by presenting the results of electro-mechanical experiments with a similar dielectric elastomer, i.e. VHB 4905^{TM} by 3M^{TM}. This polymeric material with a thickness of 500 micro-metre can show a significant amount of actuation upon the application of an electric voltage without the necessity of a pre-stretching. In an effort to model the experimental findings, an electro-viscoelastic coupled model is used that is based on our two recent contributions, i.e. a theoretical modelling framework of thermo-electro-viscoelastic problems with field dependent material parameters [1], and the second contribution investigating the visco-mechanical properties of VHB 4905^{TM} coated with an electrically conductive carbon grease [36].

This paper is organized as follows. In Section 2, the experimental setup, the sample preparation and the results of cyclic loading-unloading tests with the simultaneous application of an electric field are presented. In the following section we present a constitutive modelling approach for electro-viscoelasticity which is used in combination with the experimental results in order to identify the necessary material parameters. The final Section concludes the paper with a summary and an outlook for future works.

2 Experimental Characterization of VHB 4905

For all of the experiments presented in this contribution we use the widely-known dielectric elastomer VHB 4905^{TM} by 3M^{TM}. This is a commercially available double sided bonding tape with a thickness of 500 μm originally manufactured for adhesive applications. However, recently it has frequently been used as a dielectric elastomer due to its extreme soft mechanical properties. For electro-mechanical coupled experimentations, the material is coated on both sides with the electrically conductive carbon grease 846-80G by MG Chemicals^{TM}. All experiments are performed at constant ambient temperature of 23°C using samples of the dimensions 70 mm by 100 mm. These dimensions are selected in such a way that the ratio between the coated and the uncoated material surfaces is as large as possible while meeting the geometric constraints given by the customized experimental equipment. We perform cyclic loading-unloading tests under an electric field where the field is created by applying two opposite voltages perpendicular to the stretch direction. These experiments are conducted with the aim of identifying the material parameters from our selected finite-strain model that couples the electric field with the mechanical response of the material.

2.1 Experimental Setup

The testing equipment for the electro-mechanical experiments consists of seven major parts (c.f. Figure 2). The coated material sample (**1**) is fixed at both ends by a pair of clamps (**2**). The bottom pair is mounted on a movable table that is controlled by a linear translation stage (**3**). The top pair of clamps is connected to the force transducer (**4**) (model number GSO-1 K, Transducer Techniques) which is attached to the frame of the testing system (**5**). For the application of the electric field the coated sides of the test sample have to be connected to a power source which is achieved by a flexible electric wiring (**6**). Finally the entire setup is enclosed in a non-conductive cabinet (**7**) ensuring a safe working environment. In the loading-unloading experiments, the material samples are deformed by the movement of the table. The force that has to be applied on the sample in order to achieve the deformation is constantly recorded through the force transducer (precision limit of ±0.01 g) with a frequency of 10 data points per second. The force transducer is connected to a LabView software system. In order to ensure the reproducibility of all experiments, we conduct 5 cyclic tests for each value of the electric field. Therefore, if not stated otherwise, the results presented show an average value of the test runs which is done in order to further reduce noises. In order to characterize the experiments we use the initial length of the sample L_0 and the difference between the initial and the deformed length ΔL to define the strain $\varepsilon = \Delta L/L_0$ and the strain rate $\dot{\varepsilon} = \dot{\Delta L}/L_0$.

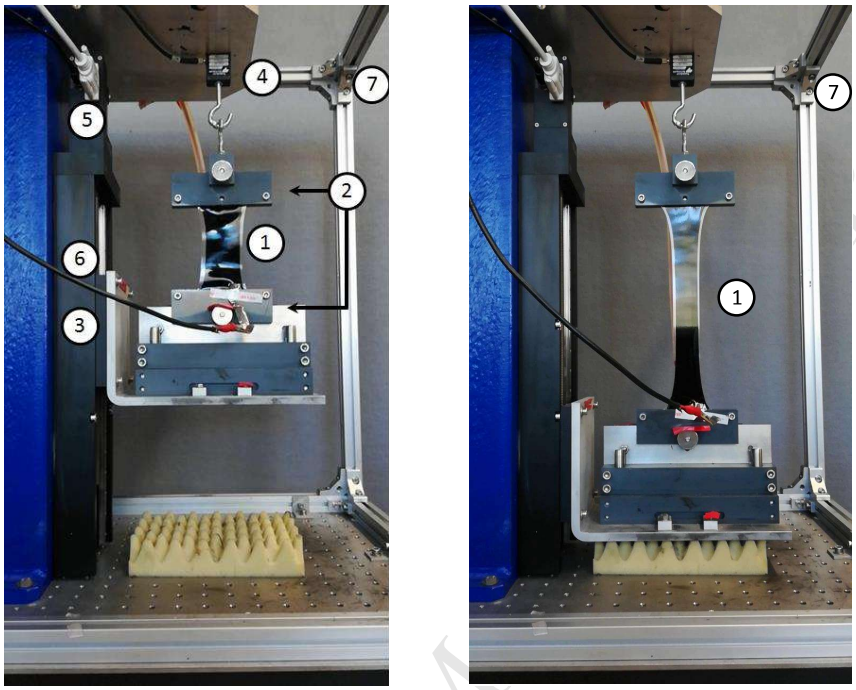

(a) Testing equipment (b) Stretched sample

Fig. 2 Coated test sample of VHB 4905^{TM} in the (a) undeformed and (b) deformed states. *Legend:* **1** coated test sample, **2** clamping plates, **3** linear stage with a movable table, **4** force transducer, **5** frame, **6** electric wiring , **7** safety cabinet.

2.2 Specimen Preparation

As explained in the previous section VHB polymers are extremely soft materials with an excellent adhesive property. Hence, it is a challenging task to prepare samples with these polymers either for purely mechanical experiments or electro-mechanically coupled tests. Therefore a simple but efficient holding frame was designed to prepare samples. Such a custom-made frame helps to paint the sample efficiently with minimum disturbances prior to the actual tests. The first step for the preparation of the test sample is to place one of the top and one of the bottom clamping plates into said holding frame. By this the distance between the top and the bottom plate is fixed at 70 mm. Therefore, the deformable length of the material sample that is held fixed by the plates is also exactly 70 mm. In the next step we carefully remove the protective covering of the VHB and put the remaining two clamping plates on top of the sample. Thanks to the bonding properties of VHB 4905^{TM}, the sample is safely fixed between the clamping plates by two pairs of screws. The next step is to cover both sides with the conductive carbon grease that acts as compliant electrodes using a soft brush. In order to prevent any short circuiting, a small area on both sides over

the entire length of the sample has to remain uncoated.

Thus in order to simplify the application of the grease, we cover an area of approximately 5 mm over the entire side lengths of the specimen with two pieces of the protective covering (Figure 3a). When the entire face of the sample is coated, the protective covering can be removed resulting in a precise and straight boundary of the coated area. We can easily check whether the the surface is completely covered by a visual examination. Next the sample and the holding frame are flipped so that the backside can also be coated with carbon grease. As the VHB investigated in this study is transparent, the line between the coated and the uncoated area on the front side is clearly visible and can be used as an orientation for the boundary during the coating of the backside. After finishing the application of the grease a stripe of aluminum foil is glued to the clamp in such a way that one end of the stripe touches the coated material whereas the other end is free to move. This ensures a flexible connection between the compliant electrode and the stiff electric cable from the power source. Finally the sample is mounted on the testing equipment and the frame is removed. Afterwards, a second stripe of aluminum foil is connected to the other side of the sample in a similar fashion so that the cable with the opposite polarization can be connected. The entire preparation process and a cyclic loading test is documented by a comprehensive and illustrative video available as supplemental material.

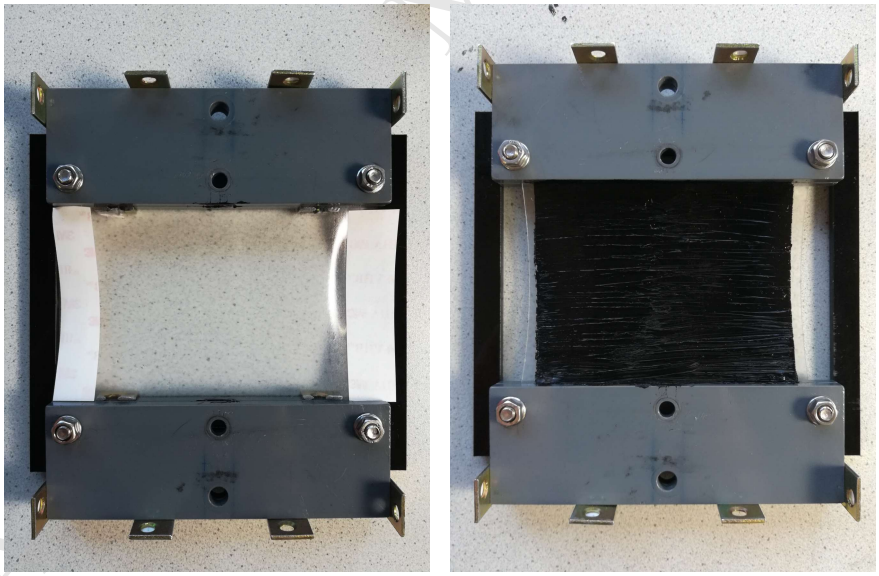

(a) Sample with protective covering on one pair of clamping plates

(b) Coated and fixed sample

Fig. 3 Clamped specimen of VHB 4905^{TM} during the sample preparation before the application of the conductive carbon grease (left) and after the application (right)

2.3 Loading-Unloading Tests

Since the loading-unloading cyclic experiments are essential and classical in characterizing viscoelastic materials, we perform a number of such tests with an electric field applied in the thickness direction of each sample. In these experiments the sample is stretched at a constant strain rate up to a maximum deformation of 200%. When the desired value of the tensile strain is reached, the stretch is immediately reduced with the same strain rate until the table of the linear stage returns to its original position. The results for three stretch velocities of 0.025 s^{-1}, 0.1s^{-1} and 0.2 s^{-1} are presented in Figs 3, 4 and 5, respectively. During the entire deformation a constant potential difference is applied between the electrodes. In order to obtain a significant influence by the electric field, we apply electric voltages of 2 kV, 3 kV, 4 kV, 5 kV and 6 kV. Additionally we perform the same tests in the absence of an electric field as reference tests. The plots in Figures 4 to 6 present the forces that are applied to the material sample during the deformation for the different stretch velocities. On the left hand side, we show the results over the entire loading cycle of 200% for the purely mechanical case (black solid line with cycles) and for a potential difference of 4kV (red solid line with crosses) and 6kV (blue solid line with triangles). On the right hand side, we present the value of the force for all of the applied voltages at the maximum applied stretch value of 200%. A dashed trend line is added for purely representation purposes and the scaling of the y-axis is adjusted is such a way that the influence of the elctric field becomes easily visible.

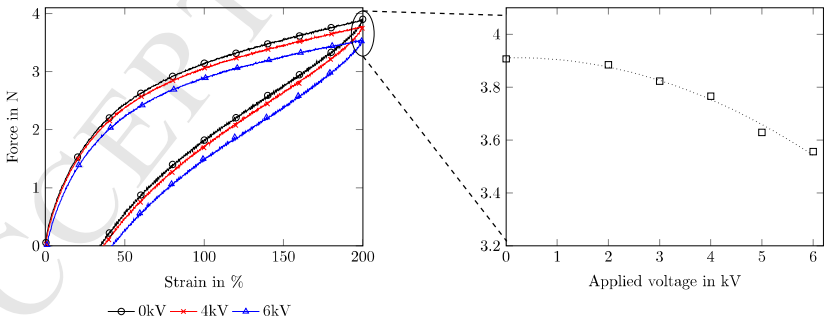

Fig. 4 Loading-unloading tests for a strain rate of $\dot{\lambda} = 0.025\ s^{-1}$. Applied force over the entire loading-unloading cycle (left). Applied force at the maximum strain value for all applied potential differences (right)

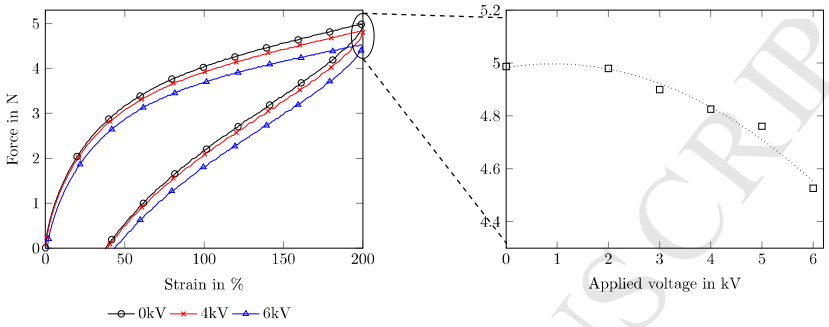

Fig. 5 Loading-unloading tests for a strain rate of $\dot{\lambda} = 0.1\ \mathrm{s}^{-1}$. Applied force over the entire loading-unloading cycle (left). Applied force at the maximum strain value for all applied potential differences (right)

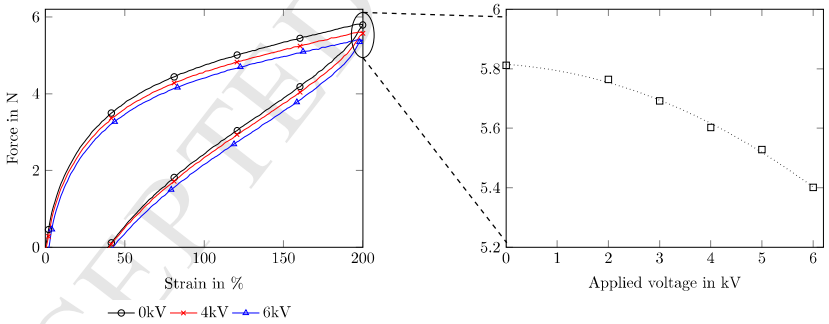

Fig. 6 Loading-unloading tests for a strain rate of $\dot{\lambda} = 0.2\ \mathrm{s}^{-1}$. Applied force over the entire loading-unloading cycle (left). Applied force at the maximum strain value for all applied potential differences (right)

From Figures (4- 6), the influence of the applied electric field on the material behavior becomes clearly visible. Independently from the stretch velocity the applied forces are reduced when a potential difference is applied and this effect becomes

more distinct the more the sample is deformed. We can see that the applied force at the maximum deformation is reduced by the application of an electric field by a percentage value of approximately 7% for the fastest deformation rate and approximately 9% for the slower deformation rates. Furthermore, the trend line suggests a nonlinear effect of the electric field on the material response. It should be noted that the influence of the applied electric field on the material response is relatively small and can not be increased significantly by the application of a higher potential difference as this leads to electric breakdown of the material. Thus for practical applications, such as soft actuators, VHB 4905^{TM} is not yet an ideal candidate. However as mentioned before, it is still an appropriate choice for simple prototypes as it is commercially available. Better results can be expected from custom made materials such as liquid silicone rubbers filled with piezoactive particles.

In our previous work on the mechanical behavior of VHB 4905^{TM} [36] and [2], in addition to cyclic experiments, a number of relaxation tests were presented as well. In such a test, a sample is rapidly deformed and held in the deformed state for a definite time period to observe the relaxed stress. However, so far these tests have not been performed successfully as the stretched material fails to sustain the high applied voltage at some points of the relaxation time. Nonetheless, an exemplary resulting curve is plotted in Figure 7. We use a sample with the same dimensions as before that is deformed with a stretch rate of 25 mm/s to a maximum deformation of 200% and is held for 30 minutes. Additionally we apply a voltage of 5 kV perpendicular to the stretch direction that is supposed to be applied until the end of the relaxation time.

In the depicted test the sample failed after approximately 550 seconds resulting in a sudden increase of the applied force which shows the vanishing influence of the electric field due to the electric breakdown.

3 Constitutive Modelling and Parameter Identification

In this section, a micro-mechanically motivated finite strain electro-viscoelastic model is presented. In a previous contribution we used the results of purely mechanical experiments to identify the necessary elastic and viscoelastic material parameters [36]. Now the model is augmented to account for the influence of the electric field on the material response.

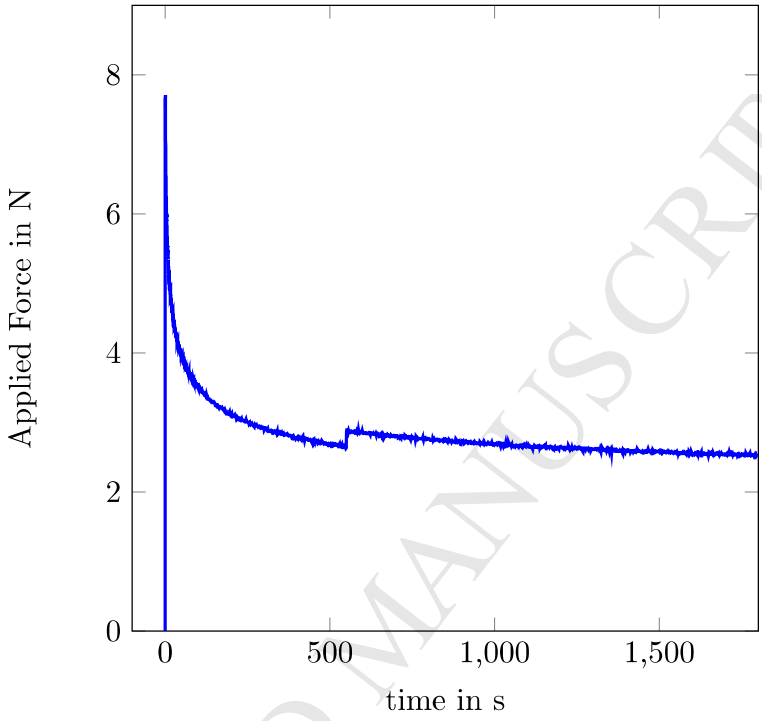

Fig. 7 Applied force during an electro-mechanical relaxation test. Electric breakdown of the material occurs at a time of approximately 550 seconds

3.1 Electro-Viscoelastic Modelling Approach

As presented in [36] the purely mechanical viscoelastic material behavior can be described using a total energy function Ψ that depends on the right Cauchy-Green tensor $\boldsymbol{C}$ and a number of internal variables $\boldsymbol{A}_i$ in the form

$$\Psi(\boldsymbol{C},\boldsymbol{A}) = \Psi_{\text{vol}}(J) + \Psi_{\text{iso}}(\overline{\boldsymbol{C}},\boldsymbol{A}) = \Psi_{\text{vol}}(J) + \Psi^{e}_{\text{iso}}(\overline{\boldsymbol{C}}) + \sum_{i=1}^{s} \Psi^{v}_{\text{iso},i}(\overline{\boldsymbol{C}},\boldsymbol{A}_i). \tag{1}$$

Here we decompose the free energy into a volumetric contribution $\Psi_{\text{vol}}(J)$ that depends on the determinant J of the deformation gradient $\boldsymbol{F}$ and into an isochoric contribution Ψ_{iso}. The latter can be further decomposed into an elastic part Ψ^{e}_{iso} that depends on the isochoric right Cauchy-Green tensor $\overline{\boldsymbol{C}} = J^{-2/3}\boldsymbol{C} = J^{-2/3}[\boldsymbol{F}^{\mathrm{T}}\boldsymbol{F}]$ and a number of viscous member functions $\Psi^{v}_{\text{iso},i}(\overline{\boldsymbol{C}},\boldsymbol{A}_i)$. Similar to Mehnert and

Steinmann [36], we select an eight-chain model for the ground state elasticity. Thus to simulate the mechanical response of the material only two material parameters, namely the shear modulus μ and the number of segments per chain N are required. Therefore, the energy function takes the form

$$\Psi^e_{\text{iso}}(\overline{\boldsymbol{C}}) = \mu N \left[\overline{\gamma}\overline{\lambda}_r + \log\left(\frac{\overline{\gamma}}{\sinh\overline{\gamma}}\right)\right], \tag{2}$$

where the inverse Langevin function $\overline{\gamma}$ is incorporated that can be approximated using the Padé approximation, i.e. $\overline{\gamma} \approx \overline{\lambda}_r \frac{3-\overline{\lambda}_r^2}{1-\overline{\lambda}_r^2}$. Furthermore, for the statistics of an individual chain we introduce the Langevin model [37] leading to a relative chain stretch $\overline{\lambda}_r = \frac{\overline{\lambda}}{\sqrt{N}} = \sqrt{\frac{\overline{I}_1}{3N}}$ with the first invariant $\overline{I}_1$ of $\overline{\boldsymbol{C}}$. Now in order to take into account the effects of the electric field $\mathbb{E}$ on the material responses, we extend this elastic energy formulation by the two coupling terms $c_1[\mathbb{E}\otimes\mathbb{E}] : \boldsymbol{I}$ and $c_2[\mathbb{E}\otimes\mathbb{E}] : \overline{\boldsymbol{C}}$ that are frequently used throughout the literature [31, 38, 39, 40]. Here the variables c_1 and c_2 are so-called coupled material parameters. Additionally, based on the results of our previous contribution [1], we introduce a field dependency of the elastic shear modulus as $\tilde{\mu}^e(\mathbb{E}) = \mu^e - \overline{\mu}^e[\mathbb{E}\otimes\mathbb{E}] : \boldsymbol{I}$, which consists of a respective ground state contribution μ^e and a coupling contribution $\overline{\mu}^e$ that depends quadratically on the applied electric field. With these additions the free energy function of an electro-elastic problem takes the form

$$\Psi^e_{\text{iso}}(\overline{\boldsymbol{C}}, \mathbb{E}) = \tilde{\mu}^e(\mathbb{E}) N \left[\overline{\gamma}\overline{\lambda}_r + \log\left(\frac{\overline{\gamma}}{\sinh\overline{\gamma}}\right)\right] + c_1[\mathbb{E}\otimes\mathbb{E}] : \boldsymbol{I} + c_2[\mathbb{E}\otimes\mathbb{E}] : \overline{\boldsymbol{C}}. \tag{3}$$

The current energy function results in a dielectric response of the material that shows a linear dependency on the electric field while also depending potentially nonlinearly on the deformation. The interested reader should note that this energy contribution can be rearranged into a purely mechanical part $\Psi^{e,\text{mech}}_{\text{iso}}(\overline{\boldsymbol{C}})$ and an electro-mechanical coupling part $\Psi^{e,\text{couple}}_{\text{iso}}(\overline{\boldsymbol{C}}, \mathbb{E})$. The latter can be formulated as

$$\Psi^{e,\text{couple}}_{\text{iso}}(\overline{\boldsymbol{C}}, \mathbb{E}) = -\frac{1}{2} J \varepsilon_0 \varepsilon_r(\overline{\boldsymbol{C}}) \overline{\boldsymbol{C}}^{-1} : [\mathbb{E}\otimes\mathbb{E}]. \tag{4}$$

In this rearranged form of the energy function the deformation dependent relative permitivity $\varepsilon_r(\overline{\boldsymbol{C}})$ contains all the coupling terms and can be rearranged into $\varepsilon_r(\boldsymbol{C}) = 1 + f(\boldsymbol{C})$. This leads to the traditional formulation consisting of a free space contribution and the contribution of the material characterized by the function $f(\boldsymbol{C})$. Thus the selected energy function yields a form that is similar to other formulations for deformation dependent electric properties [41, 42]. For the viscous energy function, we select a formulation that was introduced by Linder et al. [43] with a micro-mechanically motivated explanation as

$$\Psi^v_{\text{iso}} = \sum_{i=1}^{s} \Psi^v_{\text{iso},i}(\overline{\boldsymbol{C}}, \boldsymbol{A}_i) = \sum_{i=1}^{s} \frac{1}{2} \mu^v_i [(\boldsymbol{A}_i : \overline{\boldsymbol{C}} - 3) - \log(\det(\boldsymbol{A}_i)]. \tag{5}$$

In Equation (5), each member function of the sum represents a viscous Maxwell element containing a respective viscous shear modulus μ_i^v. Furthermore, the energy function depends on strain-like tensorial internal variables $\boldsymbol{A}_i$ which are determined by a thermodynamical consistent linear evolution law that was originally introduced by Lubliner [44]

$$\dot{\boldsymbol{A}}_i = \frac{1}{\tau_i}[\overline{\boldsymbol{C}} - \boldsymbol{A}_i], \tag{6}$$

where a relaxation time τ_i is introduced for every Maxwell element. For the parameter identification this modelling approach is implemented into an open source finite-element (FE) code using the FE library `deal.II` [45, 46].

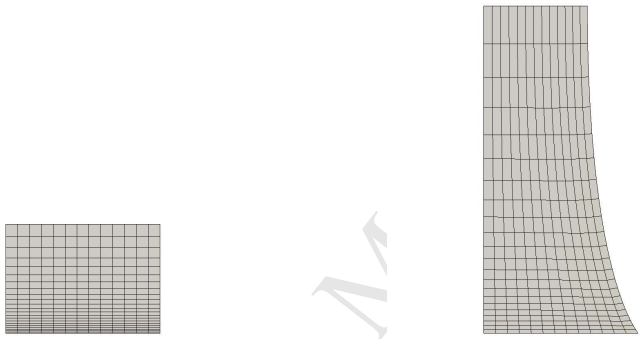

(a) Undeformed model (b) Deformed model

Fig. 8 Finite element model used in the simulation in the undeformed (left) and deformed (right) configuration. The model resembles one eighth of a sample. The rear and left cut surfaces are restrained from displacement in normal direction. The displacement of the bottom cut surface is completely fixed.

The model used in the simulation is depicted in Figure 8 in the undeformed and in the maximum deformed state. As the deformation can be assumed to be symmetric we simulate only one eighth of a real life sample in order to safe computational costs. The model is discretized with 286 eight node hexahedral elements and the displacement on the cut surfaces is fixed in zero direction. Furthermore on the bottom surface the displacement is completely fixed in order to simulate the clamping of the material in the experiment. The loading and unloading of the material is prescribed at the top surface and performed in 40 timesteps. Details on the respective variational formulation of the electro-mechanical problem and the selected solution approach can be found in our previous contribution [47] or in the works of Vogel et al. [39] or Vu et al. [40].

3.2 Parameter Identification

In a recent contribution [36] we performed an extensive experimental study on the effect of the compliant electrodes on the mechanical response of VHB 4905$^{\text{TM}}$ coated with the electrically conductive carbon grease 846-80G by MG Chemicals$^{\text{TM}}$. The results of purely mechanical, uniaxial experiments were used in combination with an analytical solution to the uniaxial problem to identify the elastic and viscous material parameters for the same material model that is used as the basis of the coupled electro-viscoelastic material model advocated in this contribution. Thus we can take the parameter values from [36] for the zero-field viscoelastic material response and use the electro-mechanical experiments for the identification of the parameters that couple the electric field with the mechanical field, i.e. $\overline{\mu}^e$ and c_2. The reader should note that the remaining material parameter c_1 does not couple the electric field with the mechanical one and can therefore not be identified using our experiments. The identified elastic and viscous material parameters taken from [36] are listed in Table 1.

μ^e	N	μ_1^v	μ_2^v	μ_3^v	μ_4^v
27.00	$7.59{\cdot}10^5$	34.27	28.02	86.47	$4.51 \cdot 10^{-4}$
		τ_1	τ_2	τ_3	τ_4
		5.69	82.97	0.81	$1.71 \cdot 10^{-3}$

Table 1 Identified material parameters. μ^e and μ_i^v in N/mm^2, τ_i in s

For the identification of the mechanical material parameters appearing in the constitutive model presented in Section 3.1, we will use a similar approach as in [36]. However, due to the more complex sample geometry and the applied boundary conditions of the electro-mechanical experiments, there is no analytical solution of the constitutive model discussed in Section 3.1. Therefore, we simulate the problem with our finite-element implementation and fit these simulation results to the experiments using a *simultaneous minimization* technique [48, 43, 36]. In this approach we sum up the errors between the simulated values of the applied force, calculated using the finite-element model and the respective experimental values for a specific combination of electric potential difference and a stretch velocity. As it is beneficial to minimize a relative expression these errors are divided by the respective experimental value. Thus for any combination of an applied stretch and an electric field we define the expression

$$\sum_{i=1}^{m} \sum_{j=1}^{n} \frac{F_{\text{sim}}^{i,j} - F_{\text{exp}}^{i,j}}{F_{\text{exp}}^{i,j}}, \tag{7}$$

as objective function. Here we have introduced the simulated value of the applied force as F_{sim}, the experimental value of the applied force as F_{exp} and i, j which are the number of stretch velocities and applied voltages that we take into consideration for

the optimization routine. The results from the finite-element analysis are handed to a nonlinear least-squares solver in Matlab. By this information exchange the optimal values of the coupling parameters are identified iteratively. As data pool for the optimization we select the maximum applied potential difference of 6 kV at all three stretch velocities 0.025 s^{-1}, 0.1s^{-1} and 0.2 s^{-1}. The reader should note that the number of experimental data sets selected for the optimization is rather small. This is neccessary as in each iteration of the optimization routine the entire problem is simulated for each configuration separately using the finite element implementation which results in a considerable runtime of the optimization. The identified values of the coupling parameters are $\overline{\mu}^e = 9.96 \cdot 10^{-12} N/(Vmm)^2$ and $c_2 = 8.96 \cdot 10^{-12} N/V^2$. Using these parameters we can now compare the experimental results with the results obtained from the finite element simulation. These results are depicted in Figures 9 -11. The plots on the left hand side show the applied force over the entire loading cycle. The results from the experiments are depicted as black circles for 0 kV and as blue triangles for 6 kV applied voltage. The results of the FE simulation are depicted in dashed lines in the according color. On the right hand side the applied force for the maximum applied stretch over the applied voltages is plotted. The results from the experiments are depicted as black squares whereas the simulation results are depicted as red crosses. For both the computational and the experimental results a dashed trend line is added for purely representation purposes and the scaling of the y-axis is adjusted is such a way that the influence of the elctric field becomes easily visible.

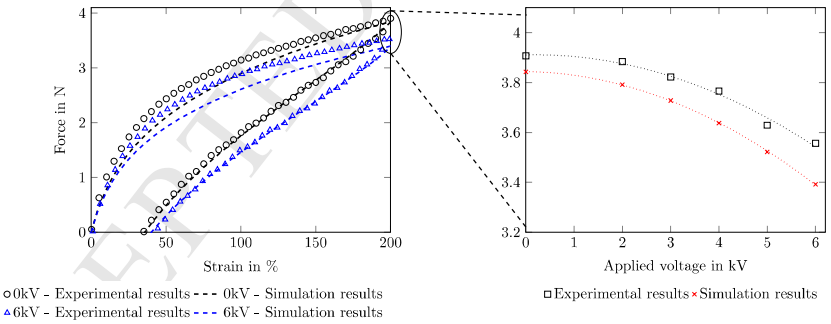

Fig. 9 Loading-unloading test for a strain rate of $\dot{\lambda} = 0.025$ s^{-1}. Applied force over the entire loading-unloading cycle (left). Applied force at the maximum stretch value for all applied potential differences (right)

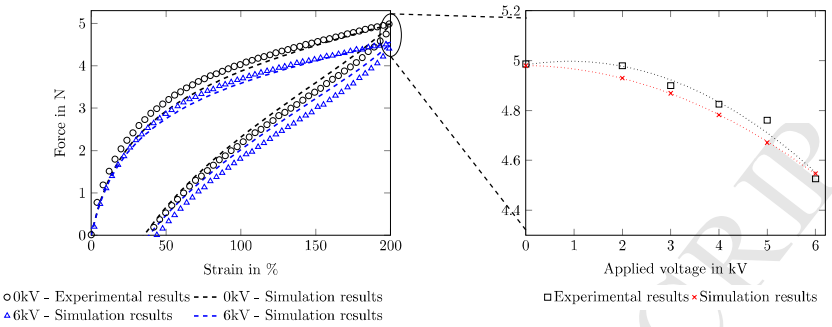

Fig. 10 Loading-unloading test for a strain rate of $\dot{\lambda} = 0.1\ \mathrm{s}^{-1}$. Applied force over the entire loading-unloading cycle (left). Applied force at the maximum strain value for all applied potential differences (right)

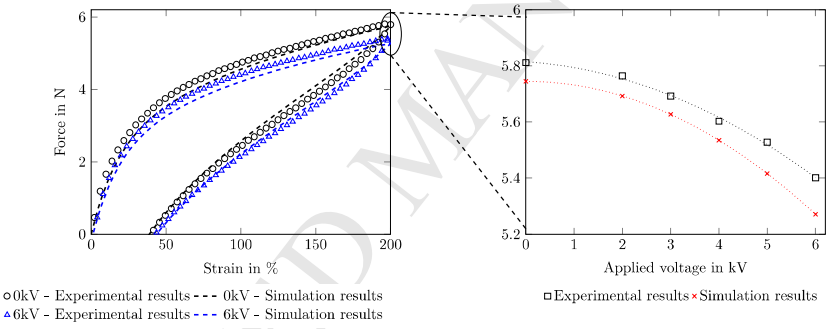

Fig. 11 Loading-unloading test for a strain rate of $\dot{\lambda} = 0.2\ \mathrm{s}^{-1}$. Applied force over the entire loading-unloading cycle (left). Applied force at the maximum strain value for all applied potential differences (right)

Given the relative simplicity of our modelling, the plots show a very good correlation between the experiments and the simulations both over the entire strain range and over the applied voltages for all of the stretch velocities. The quality of the fit can be further quantified by the calculation of the coefficient of determination R^2. It can take a value between 1, a perfect fit between the experiment and the model, and 0. It is defined as

$$R^2 = 1 - \frac{\sum_{i=1}^{n}[y_i - \hat{y}_i]^2}{\sum_{i=1}^{n}[y_i - \overline{y}]^2}. \tag{8}$$

In the definition the difference between the values of the experimental results y_i and the values of the simulation $\hat{y}_i$ are devided by the difference between the values of the experimental results and their average value $\overline{y}$. For the data presented in the

Figures 9 -11 the coefficient of determination ranges between 0.9536 and 0.9936. The curves in the left plots only show the electro-mechanical load cases that were used for the optimization routine. The minor differences in the material response especially in the beginning of the deformation result from the complex identification of the mechanical material parameters presented in [36]. In the plots on the right hand side the results from the tests that were not included in the optimization are included as well. It can be observed that the simulation also nicely replicates the experimental values of the voltages that were not used for the identification of the coupling parameters therefore validating our results.
As a further validation of our model we can also simulate the material behavior of the failed relaxation test shown in Figure 7. In order to replicate the failure of the material the electric field is switched off after 550 seconds of relaxation in the simulation. This results in a behavior as depicted in Figure 12.

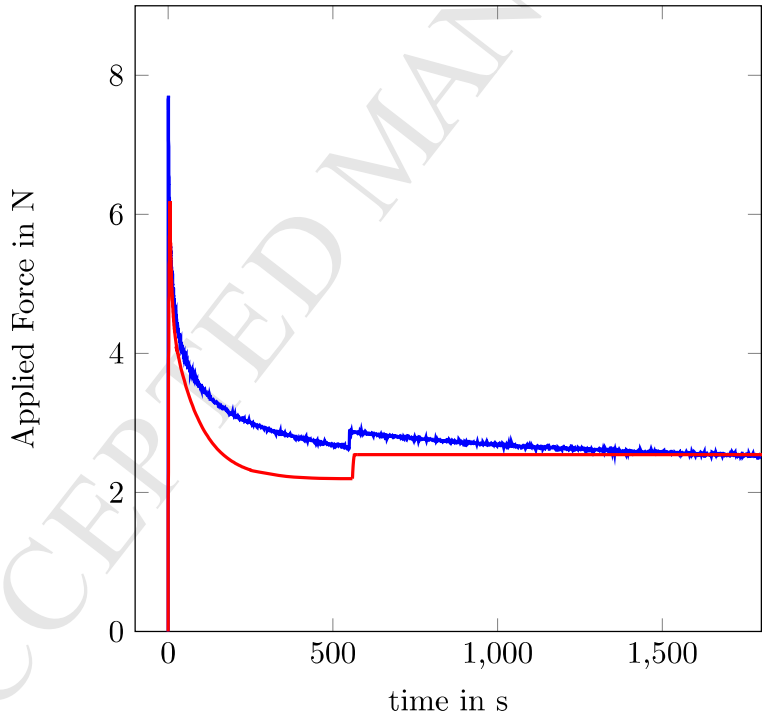

Fig. 12 Experimental results (blue line) and computational results (red line) of an electro-mechanical relaxation test. Electric breakdown of the material in the experiment and deactivation of the electric potential difference in the computation at a time of approximately 550 seconds

The experimental results are depicted as a blue solid line and the simulation as red solid line. As we can see the electro-mechanical computation simulates the material response slightly too soft resulting in a smaller applied force. Overall the material behavior is simulated satisfactorily well especially considering that the experimental graph is the result of only one single experiment. Thus the influence of possible additional effects such as the temperature or minor material variations are not canceled out by averaging. However the quality of the fitting could be increased using a more advanced viscous energy function as for example presented in [30].

4 Summary and Outlook

In the presented contribution we have examined the electro-viscoelastic material responses of the dielectric elastomer VHB 4905^{TM}. We have presented the results of loading-unloading experiments with three different stretch velocities and an electric potential difference applied perpendicular to the stretch direction. During these experiments the influence of the electric field becomes clearly visible. Furthermore we have presented an augmented finite strain viscoelastic material model that couples the viscous material response with the electric field. These experiments were used in combination with results from a previous work on the purely mechanical behavior for the identification of the coupling material parameters of the model. Finally we use a finite-element implementation to replicate the experimental results using the identified parameters. For our future work, we aim to conduct similar experiments with various temperatures thus ultimately providing a complete thermo-electro-viscoelastic characterization of VHB 4905^{TM}. Also the influence of an quantifiable applied pre-stretch on the electro-mechanical material response should be adressed in future contributions. Furthermore this characterization will also be performed for different materials such as silicones filled with piezoactive particles that amplify the electro-mechanical coupling.

Acknowledgements:
M. Mehnert acknowledges the funding within the DFG project No. STE 544/52-2. M. Hossain acknowledges Swansea University support with the new staff fund EGD1005-209 that facilitated an exchange visit of the first author at Zienkiewicz Centre for Computational Engineering (ZCCE).

References

1. M. Mehnert, M. Hossain, and P. Steinmann, “Numerical modeling of thermo-electro-viscoelasticity with field-dependent material parameters,” *International Journal of Non-Linear*

Mechanics, vol. 106, pp. 13–24, 2018.
2. M. Hossain, D. K. Vu, and P. Steinmann, "A comprehensive characterization of the electro-mechanically coupled properties of vhb 4910 polymer," *Archive of Applied Mechanics*, vol. 85, no. 4, pp. 523–537, 2015.
3. F. Carpi *et al.*, *Electromechanically active polymers*. Springer, 2016.
4. L. Maffli, S. Rosset, M. Ghilardi, F. Carpi, and H. Shea, "Ultrafast all-polymer electrically tunable silicone lenses," *Advanced Functional Materials*, vol. 25, no. 11, pp. 1656–1665, 2015.
5. M. Blum, M. Büeler, C. Grätzel, J. Giger, and M. Aschwanden, "Optotune focus tunable lenses and laser speckle reduction based on electroactive polymers," in *Moems and Miniaturized Systems Xi*, vol. 8252, p. 825207, International Society for Optics and Photonics, 2012.
6. A. K. Price and C. T. Culbertson, "Generation of nonbiased hydrodynamic injections on microfluidic devices using integrated dielectric elastomer actuators," *Analytical chemistry*, vol. 81, no. 21, pp. 8942–8948, 2009.
7. D. McCoul, C. Murray, D. Di Carlo, and Q. Pei, "Dielectric elastomer actuators for active microfluidic control," in *Electroactive Polymer Actuators and Devices (EAPAD) 2013*, vol. 8687, p. 86872G, International Society for Optics and Photonics, 2013.
8. A. O'Halloran, F. O'malley, and P. McHugh, "A review on dielectric elastomer actuators, technology, applications, and challenges," *Journal of Applied Physics*, vol. 104, no. 7, p. 9, 2008.
9. Y. Bar-Cohen, "Electroactive polymers: current capabilities and challenges," in *SPIE's 9th Annual International Symposium on Smart Structures and Materials*, pp. 1–7, International Society for Optics and Photonics, 2002.
10. Y. Bar-Cohen, *Electroactive polymer (EAP) actuators as artificial muscles: reality, potential, and challenges*, vol. 136. SPIE press, 2004.
11. R. Vertechy, M. Fontana, G. R. Papini, and D. Forehand, "In-tank tests of a dielectric elastomer generator for wave energy harvesting," in *SPIE Smart Structures and Materials+ Nondestructive Evaluation and Health Monitoring*, pp. 90561G–90561G, International Society for Optics and Photonics, 2014.
12. H. Böse and E. Fuß, "Novel dielectric elastomer sensors for compression load detection," in *SPIE Smart Structures and Materials+ Nondestructive Evaluation and Health Monitoring*, pp. 905614–905614, International Society for Optics and Photonics, 2014.
13. S. J. A. Koh, C. Keplinger, T. Li, S. Bauer, and Z. Suo, "Dielectric elastomer generators: How much energy can be converted?," *IEEE/ASME Transactions on mechatronics*, vol. 16, no. 1, pp. 33–41, 2011.
14. J. Biggs, K. Danielmeier, J. Hitzbleck, J. Krause, T. Kridl, S. Nowak, E. Orselli, X. Quan, D. Schapeler, W. Sutherland, *et al.*, "Electroactive polymers: developments of and perspectives for dielectric elastomers," *Angewandte Chemie International Edition*, vol. 52, no. 36, pp. 9409–9421, 2013.
15. P. Brochu and Q. Pei, "Advances in dielectric elastomers for actuators and artificial muscles," *Macromolecular rapid communications*, vol. 31, no. 1, pp. 10–36, 2010.
16. S. Rosset and H. R. Shea, "Flexible and stretchable electrodes for dielectric elastomer actuators," *Applied Physics A*, vol. 110, no. 2, pp. 281–307, 2013.
17. R. Pelrine, R. Kornbluh, J. Joseph, R. Heydt, Q. Pei, and S. Chiba, "High-field deformation of elastomeric dielectrics for actuators," *Materials Science and Engineering: C*, vol. 11, no. 2, pp. 89–100, 2000.
18. R. D. Kornbluh, R. Pelrine, J. Joseph, R. Heydt, Q. Pei, and S. Chiba, "High-field electrostriction of elastomeric polymer dielectrics for actuation," in *Smart Structures and Materials 1999: Electroactive Polymer Actuators and Devices*, vol. 3669, pp. 149–162, International Society for Optics and Photonics, 1999.
19. M. Benslimane, P. Gravesen, and P. Sommer-Larsen, "Mechanical properties of dielectric elastomer actuators with smart metallic compliant electrodes," in *Smart structures and materials 2002: Electroactive polymer actuators and devices (EAPAD)*, vol. 4695, pp. 150–158, International Society for Optics and Photonics, 2002.
20. A. C. Eringen, "On the foundations of electroelastostatics," *International Journal of Engineering Science*, vol. 1, no. 1, pp. 127–153, 1963.

21. H. Allik and T. J. Hughes, "Finite element method for piezoelectric vibration," *International journal for numerical methods in engineering*, vol. 2, no. 2, pp. 151–157, 1970.
22. Y. Kagawa and T. Yamabuchi, "Finite element simulation of two-dimensional electromechanical resonators," *IEEE Transactions on Sonics and Ultrasonics*, vol. 21, no. 4, pp. 275–282, 1974.
23. A. Dorfmann and R. Ogden, "Nonlinear electroelasticity," *Acta Mechanica*, vol. 174, no. 3-4, pp. 167–183, 2005.
24. A. Dorfmann and R. Ogden, "Nonlinear electroelastic deformations," *Journal of Elasticity*, vol. 82, no. 2, pp. 99–127, 2006.
25. L. Dorfmann and R. W. Ogden, "Nonlinear electroelasticity: material properties, continuum theory and applications," in *Proc. R. Soc. A*, vol. 473, p. 20170311, The Royal Society, 2017.
26. G. A. Holzapfel and J. C. Simo, "A new viscoelastic constitutive model for continuous media at finite thermomechanical changes," *International Journal of Solids and Structures*, vol. 33, no. 20-22, pp. 3019–3034, 1996.
27. M. Kaliske and H. Rothert, "Formulation and implementation of three-dimensional viscoelasticity at small and finite strains," *Computational Mechanics*, vol. 19, no. 3, pp. 228–239, 1997.
28. J. C. Simo, "On a fully three-dimensional finite-strain viscoelastic damage model: formulation and computational aspects," *Computer methods in applied mechanics and engineering*, vol. 60, no. 2, pp. 153–173, 1987.
29. N. Huber and C. Tsakmakis, "Finite deformation viscoelasticity laws," *Mechanics of materials*, vol. 32, no. 1, pp. 1–18, 2000.
30. S. Reese and S. Govindjee, "A theory of finite viscoelasticity and numerical aspects," *International journal of solids and structures*, vol. 35, no. 26-27, pp. 3455–3482, 1998.
31. A. Ask, A. Menzel, and M. Ristinmaa, "Phenomenological modeling of viscous electrostrictive polymers," *International Journal of Non-Linear Mechanics*, vol. 47, no. 2, pp. 156–165, 2012.
32. A. Ask, A. Menzel, and M. Ristinmaa, "Electrostriction in electro-viscoelastic polymers," *Mechanics of Materials*, vol. 50, pp. 9–21, 2012.
33. A. Büschel, S. Klinkel, and W. Wagner, "Dielectric elastomers–numerical modeling of nonlinear visco-electroelasticity," *International Journal for Numerical Methods in Engineering*, vol. 93, no. 8, pp. 834–856, 2013.
34. P. Saxena, M. Hossain, and P. Steinmann, "A theory of finite deformation magneto-viscoelasticity," *International Journal of Solids and Structures*, vol. 50, no. 24, pp. 3886–3897, 2013.
35. M. Hossain, D. K. Vu, and P. Steinmann, "Experimental study and numerical modelling of vhb 4910 polymer," *Computational Materials Science*, vol. 59, pp. 65–74, 2012.
36. M. Mehnert and P. Steinmann, "On the influence of the compliant electrodes on the mechanical behavior of vhb 4905," *Computational Materials Science*, vol. 160, pp. 287–294, 2019.
37. E. M. Arruda and M. C. Boyce, "A three-dimensional constitutive model for the large stretch behavior of rubber elastic materials," *Journal of the Mechanics and Physics of Solids*, vol. 41, no. 2, pp. 389–412, 1993.
38. R. Bustamante, "Transversely isotropic nonlinear magneto-active elastomers," *Acta mechanica*, vol. 210, no. 3-4, pp. 183–214, 2010.
39. F. Vogel, *On the Modeling and Computation of Electro-and Magneto-active Polymers*. Lehrstuhl für Technische Mechanik, Universität Erlangen-Nürnberg, 2015.
40. D. Vu, "A study on nonlinear electro-elastostatics: Theory and numerical simulation," *Habilitation, Friedrich-Alexander University of Erlangen-Nürnberg: Erlangen, Bayern, Germany*, 2014.
41. D. Bishara and M. Jabareen, "A reduced mixed finite-element formulation for modeling the viscoelastic response of electro-active polymers at finite deformation," *Mathematics and Mechanics of Solids*, p. 1081286518802419, 2018.
42. A. Ask, A. Menzel, and M. Ristinmaa, "Modelling of viscoelastic dielectric elastomers with deformation dependent electric properties," *Procedia Iutam*, vol. 12, pp. 134–144, 2015.

43. C. Linder, M. Tkachuk, and C. Miehe, "A micromechanically motivated diffusion-based transient network model and its incorporation into finite rubber viscoelasticity," *Journal of the Mechanics and Physics of Solids*, vol. 59, no. 10, pp. 2134–2156, 2011.
44. J. Lubliner, "A model of rubber viscoelasticity," *Mechanics Research Communications*, vol. 12, no. 2, pp. 93–99, 1985.
45. W. Bangerth, R. Hartmann, and G. Kanschat, "deal. ii - a general-purpose object-oriented finite element library," *ACM Transactions on Mathematical Software (TOMS)*, vol. 33, no. 4, p. 24, 2007.
46. W. Bangerth, T. Heister, L. Heltai, G. Kanschat, M. Kronbichler, M. Maier, B. Turcksin, and T. D. Young, "The deal. ii library, version 8.2," *Archive of Numerical Software*, vol. 3, no. 100, pp. 1–8, 2015.
47. M. Mehnert, J.-P. Pelteret, and P. Steinmann, "Numerical modelling of nonlinear thermo-electro-elasticity," *Mathematics and Mechanics of Solids*, vol. 22, no. 11, pp. 2196–2213, 2017.
48. A. Amin, M. Alam, and Y. Okui, "An improved hyperelasticity relation in modeling viscoelasticity response of natural and high damping rubbers in compression: experiments, parameter identification and numerical verification," *Mechanics of materials*, vol. 34, no. 2, pp. 75–95, 2002.

Highlights

- We present a number of real-life electro-mechanical experiments with the dielectric elastomer VHB 4905™.
- A modelling approach for electro-viscoelasticity with field dependent material parameters is presented.
- The results of the experiments are used for the identification of the material parameters using an optimization routine in combination with a finite-element implementation.